Curve Motion Constraint Equation and its Applications

Shaogang Gong

Robotics Research Group, Oxford University, England

Abstract

In order to understand the parallel computation of optic flow, we introduce here a novel algorithm to compute the flow field at certain locations in the image. These locations are on the gradient edges, which Brady calls *seeds* [1]. Our Curve Motion Constraint Equation gives us an additional constraints to fully and locally estimate the flow field at seeds. Our initial computational experiments have used the improved local flow as the initial input to Hildreth's algorithm. Now we are exploring an algorithm to perform the whole computation in parallel.

1 Introduction

Horn and Schunck introduced the motion constraint equation to compute "optic flow", which is an apparent visual motion field in a two--dimensional successive image sequence. The equation corresponds to a first order Taylor's series expansion of the image intensity function [9]. As it only provides one constraint on the optic flow vector at any position in the image, "aperture problem" exists in the computation. In order to fully constrain or estimate the optic flow, Horn and Schunck introduced an assumption that the physical world is locally smooth everywhere, as is the optic flow. By using the smoothness assumption to regularise the flow field (to achieve global minimisation), they suggested that the aperture problem can be overcome [9]. Under egomotions in which the camera moves against a static environment, the optic flow seems to be smooth everywhere. But in a general situation which the image contains at least one moving object against a static background, the flow won't be smooth. Also, depth discontinuities give rise to two-dimensional motion field discontinuities [21], [20], [5]. To avoid the two-dimensional, namely all directions, smoothness assumption in the image, some other algorithms have been investigated [3], [24], [23], [26], [21], [20]. Hildreth's scheme [7] only smoothes the flow along one-dimensional curves corresponding to the zero crossings of the image. The arguments for doing so are based on: physiological evidences [8], the numerical conditioning of the motion constraint equation and, the physical adequacy for assuming the smoothness along edges rather than everywhere in the image. Hildreth's approach is supported by some experimental results [8], [5]. Though it is clearly one of the best schemes proposed for estimating optic flow (at least along curves), it is inherently sequential [5]. Alternatively, Scott's Four Line Method [21] computes a dense optic flow similar to that of Horn and Schunck, but he argues that the flow field across a motion boundary won't be smoothed out by his scheme and, furthermore, the match procedure being used is a local mechanism instead of a global regularisation. Therefore, it overcomes the sequential computation problem associated with Hildreth. In practice, compare with Horn and Schunck's method, the four line algorithm improves the computation of a discontinuous flow field caused by the discontinuity of the three-dimensional depth of the object. But the match scheme employed in the algorithm tends to propagate the flow field into the static background region which has any local edge structure. This gives the effect of a "wake" surrounding moving objects, although it employs the novel idea of combining different kinds of motion computation within a single scheme [5].

Imposing observational assumptions, such as smoothness, about the physical world, are aimed at overcoming the aperture problem by introducing another constraint. But how has this additional constraint been established? Most people simply apply regularisation to achieve a global minimisation. There are hardly ideas about trying to find a local constraint which is able to let us fully estimating the flow by only involving local computation. Koenderinck has carried out some theoretical investigations from biological point of view [11], [12], [10]. In computer vision, work has been carried out by Nagel in his second order Taylor series expansion of the intensity function. Nagel showed that at grey value corners, the full flow can be computed by his second order equation [14]. More recently, Nagel shows that employing the smoothness assumption along the edges, such as Hildreth, or other kinds of 'oriented smoothness' assumptions are implicitly employing the higher order of Taylor expansion of the intensity function [15]. Theoretically as well as practically, we have been inspired by Nagel's work [14], [13], [15].

The work represented in this paper is to understand the degree of constraint on the optic flow computation at the seed locations as we will describe later [1], [4]. We claim that at the seed locations, we can obtain an additional local constraint to fully estimate the optic flow locally.

2 Seeds and its constraints

Seeds are locations of two-dimensional constraint [1], examples of which include Nagel's grey value corners, or other kinds of models based on the changes of second order derivatives of the intensity function [6], [17], [16], etc. At seed locations, we have two-dimensional constraint on the flow vector which means that in theory, we can fully estimate the flow locally. This observation has been noted previously [13], [15], [1]. In fact, in the case of estimating so called *long range motion* [22], by which first computing some kinds of token, such as a corner, and then matching these tokens to give a sparse flow in the image, is applying this concept *implicitly*. Less work has been carried out in the case of computing optic flow which can provide a denser flow field for three--dimensional structure from motion. The question we addressed here is to ask what kind of reliable and local constraint on the optic flow we can get at the seed locations, in which order to support the parallel edge motion computation.

Instead of trying to recover the optic flow field everywhere in the image by a single mechanism, we believe that there are different schemes associated with different intensity structures for estimating the flow. In an image, there are loci of different constraints, such as points within

regions of smooth change or constant intensity value, points of one-dimensional intensity discontinuity which are often associated with edges, and points of two-dimensional intensity discontinuity which are seeds. According to the degree of the constraint, there are degrees of locality. There are loci in the image at which we can completely and locally compute the optic flow without global assumptions. But as the constraint decreasing, we need different scheme to estimate the flow which can not be computed locally. Therefore, the parallel computation of two-dimensional apparent motion can not be employed through out all the stages of the computation. It suggests that the computation of the optic flow should be a multi-level mechanism in the sense that different levels are associated with a certain degree of well-conditioning as well as of parallelism. The solution to the question of parallel computation of visual motion is to maximally employ the degree of parallelism which are different in different stages of the computation, instead of trying to employ a single parallel computation mechanism all the way through. Similar suggestions are to be found in physiological and psychological experiments [18], [19].

3 Mathematical structure for the seed's flow

The conditions in which we can locally compute both components of the optic flow along an edge has been studied mathematically and, it leads to an algorithm which has been implemented. Our initial computational experiments have simply used the improved local flow estimated as input to an improved Hildreth's algorithm. The results from the experiments have shown us how a new algorithm, which will perform an entire computation in parallel, can be designed.

We start from the ***Motion Constraint Equation*** (m.c.e.):

$$\nabla \mathbf{I} \cdot \mu + I_t = 0 \tag{1}$$

which derives from the assumption of temporally constant intensity. In the equation, $\nabla \mathbf{I}$ is the first order spatial gradient. μ is the optic flow vector, defined as:

$$\mu = \left[\begin{array}{cc} dx/dt & dy/dt \end{array} \right]^{\mathsf{T}} \tag{2}$$

and I_t is the temporal gradient at a pixel. The relationship between the spatial, temporal gradients and the optic flow vector is then:

$$\mathbf{N} \cdot \mu = -\frac{I_t}{\|\nabla I\|} \tag{3}$$

where $\mathbf{N} = \nabla \mathbf{I}/\|\nabla I\|$ is the unit vector in the direction of the spatial gradient.

Equation 3 imposes one local constraint on the flow vector, but if the norm of spatial gradient $\|\nabla I\|$ is small, the computation will also be poorly-conditioned. This is exactly the numerical argument in favour of edge motion estimation proposed by Hildreth. Therefore, we restrict our attention to those image loci, ***edges***, where exist high first-order spatial gradient ($\nabla^2 \mathbf{I} = 0$). At such an edge point, an ***edgel***, the intensity gradient is orthogonal (in the image plane) to the (tangent to the) edge.

If we examine an edge in a temporal sequence of images, we'll notice that in one representation, edgels are addressed by their image coordinates (x, y); and in another representation, the same point is accessed by its distance s along the edge. Add the time parameter t, we denote the quantities that feature in our analysis as follows:

$I(x, y, t)$:	intensity of a pixel.
$I(s, t)$:	intensity of an edgel.
$\gamma(s, t)$:	an edge.
$x(s, t)$:	x coordinate of an edgel.
$y(s, t)$:	y coordinate of an edgel.
$\nabla \mathbf{I}$:	spatial gradient of a pixel.
$\mathbf{N}$:	unit vector in the gradient direction.
$\mathbf{T}$:	unit vector orthogonal to $\mathbf{N}$.
μ :	velocity vector of a pixel.
$\mathbf{H}$:	Hessian matrix of a pixel.

The position along an edge is given by s. At any instant time t_i, and at any particular point on the curve, we have:

$$\mathbf{T} = \frac{\partial \gamma}{\partial s}|_{t=t_i} \quad where \quad \gamma = \gamma(s, t)$$

In other wards:

$$\mathbf{T} = \left[\begin{array}{cc} \partial x/\partial s & \partial y/\partial s \end{array} \right]^{\mathsf{T}} \tag{4}$$

After the statements have been cleared, it can be shown what the tangential component of the flow vector along an edge should be. First we have the Taylor expansion of the optic flow along an edge:

$$\mu(s + \Delta s) = \mu(s) + \frac{\partial \mu}{\partial s}\Delta s + \frac{\partial^2 \mu}{\partial s^2}\Delta s^2 + O(\Delta s^3)$$

Similarly, the Taylor expansion of $\nabla \mathbf{I}$ and I_t along an edge should be :

$$\nabla \mathbf{I}(s + \Delta s) = \nabla \mathbf{I}(s) + \frac{\partial \nabla \mathbf{I}}{\partial s}\Delta s + \frac{\partial^2 \nabla \mathbf{I}}{\partial s^2}\Delta s^2 + O(\Delta s^3)$$

$$I_t(s + \Delta s) = I_t(s) + \frac{\partial I_t}{\partial s}\Delta s + \frac{\partial^2 I_t}{\partial s^2}\Delta s^2 + O(\Delta s^3)$$

Ignore the triple and higher order of Δs in the above equations, we have:

$$\mu(s + \Delta s) = \mu(s) + \frac{\partial \mu}{\partial s}\Delta s + \frac{\partial^2 \mu}{\partial s^2}\Delta s^2 \tag{5}$$

$$\nabla \mathbf{I}(s + \Delta s) = \nabla \mathbf{I}(s) + \frac{\partial \nabla \mathbf{I}}{\partial s}\Delta s + \frac{\partial^2 \nabla \mathbf{I}}{\partial s^2}\Delta s^2 \tag{6}$$

and

$$I_t(s + \Delta s) = I_t(s) + \frac{\partial I_t}{\partial s}\Delta s + \frac{\partial^2 I_t}{\partial s^2}\Delta s^2 \tag{7}$$

Consider the m.c.e. in the neighbourhood of an edgel at distance s along the edge, which is:

$$\nabla \mathbf{I}(s + \Delta s) \cdot \mu(s + \Delta s) + I_t(s + \Delta s) = 0 \tag{8}$$

Therefore, substitute equations 5, 6 and 7 into this neighbourhood m.c.e.; then ignoring the triple and higher order of Δs gives:

$$\begin{aligned} &(\nabla \mathbf{I} \cdot \mu + I_t) + (\nabla \mathbf{I} \cdot \frac{\partial \mu}{\partial s} + \frac{\partial \nabla \mathbf{I}}{\partial s} \cdot \mu + \frac{\partial I_t}{\partial s})\Delta s \\ &+(\frac{\partial \nabla \mathbf{I}}{\partial s} \cdot \frac{\partial \mu}{\partial s} + \mu \frac{\partial^2 \nabla \mathbf{I}}{\partial s^2} + \nabla \mathbf{I} \cdot \frac{\partial^2 \mu}{\partial s^2} + \frac{\partial^2 I_t}{\partial s^2})(\Delta s)^2 \quad = \quad 0 \end{aligned}$$

The partial derivatives of intensity and velocity with respect to a spatial coordinate are constant. Therefore, to satisfy the above equation, the coefficients of zero, first and second order in Δs should respectively be 0. This leads to:

$$\nabla \mathbf{I} \cdot \mu + I_t = 0 \tag{9}$$

$$\nabla \mathbf{I} \cdot \frac{\partial \mu}{\partial s} + \frac{\partial \nabla \mathbf{I}}{\partial s} \cdot \mu + \frac{\partial I_t}{\partial s} = 0 \tag{10}$$

and

$$\frac{\partial \nabla \mathbf{I}}{\partial s} \cdot \frac{\partial \mu}{\partial s} = 0 \tag{11}$$

Equation 9 is the m.c.e.. Equations 10 and 11 provide two new relationships between the intensity and the flow along an edge. What do equation 10 and 11 tell us ?

Applying the two different coordinate representations introduced before, will lead equation 10 and 11 into:

$$(\mathbf{T}^{\mathsf{T}}\mathbf{H}\mathbf{N})(\mathbf{N} \cdot \mu) + (\mathbf{T}^{\mathsf{T}}\mathbf{H}\mathbf{T})(\mathbf{T} \cdot \mu) - (\mathbf{T}^{\mathsf{T}}\mathbf{H}\mu) = 0 \tag{12}$$

and

$$(\mathbf{T}^\top \mathbf{HN})\{(\mathbf{T}^\top \mathbf{H}\mu) + (\nabla \mathbf{I_t} \cdot \mathbf{T})\} = 0. \quad (13)$$

respectively (the detailed proof can be found in the Appendix). Where $\nabla \mathbf{I_t}$ is the temporal gradient of the spatial gradient. Clearly, equation 12 provides no additional information. However, equation 13 links the tangential and normal components of the optic flow along the edge. This will be seen in more detail from the following.

From equation 13, we have either:

$$\mathbf{T}^\top \mathbf{HN} = 0 \quad or \quad (\mathbf{T}^\top \mathbf{H}\mu) + (\nabla \mathbf{I_t} \cdot \mathbf{T}) = 0$$

If $(\mathbf{T}^\top \mathbf{HN})$ is zero, then either $\mathbf{HT}$ is parallel to $\mathbf{T}$ or, is $\mathbf{0}$. Now:

$$\begin{aligned} \frac{\partial \nabla \mathbf{I}}{\partial s} &= \frac{\partial \|\nabla I\|}{\partial s}\mathbf{N} + \|\nabla I\|\frac{\partial \mathbf{N}}{\partial s} \\ &= (\mathbf{T}^\top \mathbf{HN})\mathbf{N} + (\mathbf{T}^\top \mathbf{HT})\mathbf{T} = \mathbf{HT} \end{aligned}$$

So, *in general*, $(\mathbf{HT})$ is not parallel to $\mathbf{T}$, nor is it equal to $\mathbf{0}$. In other words, generally we have the *Curve Motion Constraint Equation* (c.m.c.e) as the following:

$$(\mathbf{T}^\top \mathbf{HN})(\mathbf{N} \cdot \mu) + (\mathbf{T}^\top \mathbf{HT})(\mathbf{T} \cdot \mu) = -(\nabla \mathbf{I_t} \cdot \mathbf{T}) \quad (14)$$

Is there any special case for which $\mathbf{T}^\top \mathbf{HN}$ vanishes? As:

$$(\mathbf{T}^\top \mathbf{HN})\mathbf{N} + (\mathbf{T}^\top \mathbf{HT})\mathbf{T} = \mathbf{HT}$$

which means if,

$$\mathbf{T}^\top \mathbf{HN} = 0 \quad \Rightarrow \quad \mathbf{HT} = (\mathbf{T}^\top \mathbf{HT})\mathbf{T}$$

As we have:

$$\kappa = -\frac{1}{\|\nabla I\|}(\mathbf{T}^\top \mathbf{HT})$$

which κ is the curvature of the edge, therefore:

$$\mathbf{HT} = -\kappa \|\nabla I\| \mathbf{T}$$

If $\mathbf{HT}$ is parallel to $\mathbf{T}$, $\mathbf{T}^\top \mathbf{HN}$ equals to 0. In fact, we found analytically that this situation happens along a circular edge. This may explain why we can not compute a circular object's rotation about its centre, for which all the full flow vectors on the edge only have tangential component.

Except for the case that $\mathbf{HT}$ is parallel to $\mathbf{T}$, furthermore, being 0 — in other words, edge is a straight line, also makes $\mathbf{T}^\top \mathbf{HN}$ vanishing. This gives:

$$\mathbf{0} = \begin{bmatrix} \partial I_x/\partial s & \partial I_y/\partial s \end{bmatrix}^\top = \mathbf{HT} \quad (15)$$

which means that both $\partial I_x/\partial s$ and $\partial I_y/\partial s$ are equal to zero. It gives the following:

1. At first, equation 15 can be more explicitly written as:

$$\mathbf{0} = \mathbf{HT} = \frac{1}{\|\nabla I\|}\begin{bmatrix} I_{xx}I_y - I_{xy}I_x \\ I_{xy}I_y - I_{yy}I_x \end{bmatrix} \quad (16)$$

namely,

$$I_{xx}I_y - I_{xy}I_x = 0, \quad I_{xy}I_y - I_{xy}I_x = 0$$

This obviously gives us: $I_{xx}I_{yy} = I_{xy}^2$. Therefore, where the edge is straight, we have:

$$det\mathbf{H} = 0$$

2. Secondly, as:

$$(\mathbf{T}^\top \mathbf{H}\mu) + (\nabla \mathbf{I_t} \cdot \mathbf{T}) = (\nabla \mathbf{I_t} \cdot \mathbf{T}) \neq 0$$

which means where the edge is straight, c.m.c.e doesn't hold.

By this stage, we have determined a relationship between the edge's optic flow and the corresponding intensity structure. This can be briefly summaried as:

conditions if we assume: *in general, the second order derivatives of the intensity function exist locally*, then we have:

1. To require an edge being straight, means that the determinant of the local *Hessian* matrix equals to zero.
2. Theoretically, we can estimate both components of optic flow locally along edges wherever the edge is not straight, though we still can not estimate the circular objects rotating according to its centre. Practically, we need to concern ourselves with the numerical condition of the c.m.c.e.. It is very similar to the situation that arises in using the m.c.e.. For the m.c.e., it is judged by the norm of the gradient. For the c.m.c.e., it is judged by $det\mathbf{H}$. In fact, $det\mathbf{H} = \kappa_1\kappa_2(EG - F^2)$, in which E, F and G are the components of the first fundamental form [17], which suggested that the intensity surface shape can be basically classified into three types based on the value of $det\mathbf{H}$. That is:

   $det\mathbf{H} < 0$, hyperbolic point;
   $det\mathbf{H} > 0$, elliptic point;
   $det\mathbf{H} = 0$, parabolic point.

   The parabolic points are associated with the straight edges in the intensity surface, but both hyperbolic and elliptic points are associated with seed locations.
3. Furthermore, where the $det\mathbf{H}$ equals to zero, the optic flow estimation reverts to be an under-determined problem.

What can deduce from the c.m.c.e. ? First of all, we can write the c.m.c.e. in a more general form as: $\phi(\mathbf{T} \cdot \mu) + \varphi(\mathbf{N} \cdot \mu) + \lambda = 0$. So the equation gives the correct solution in two kinds of extreme situations (figure 1).

Secondly, we see that Hessian matrix plays a central role here. In practice, we only can compute the $\mathbf{T} \cdot \mu$ where $\mathbf{H}$ is well-conditioned. $\mathbf{H}$ is associated with the surface curvature of the intensity function [25], [14], [17]. In fact, large Hessian determinant is associated with the loci of local maximum surface curvature on the intensity surface, which are the loci of two-dimensional constraint. Therefore, they correspond

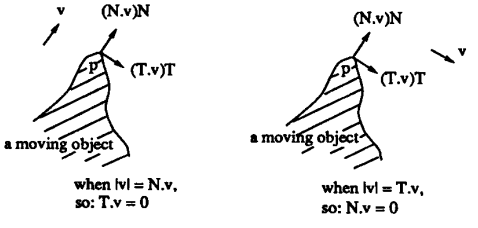

Figure 1: Two extreme situations for the flow field computation.

to the loci of seeds, where we can give a full value for the optic flow. Though it seems to be similar to Nagel's *grey value corners*, we derived here an explicit connection between the structure of intensity on the edge and the constraint for computing the optic flow at these locations. This connection generalises Nagel's method by giving explicit detail about not only dealing with the flow of two-dimensional constraint loci — grey value corners; but also dealing with the flow of one-dimensional constraint loci — edges, and about the degree of numerical reliability for local flow computation on these edges.

4 Improved local flow for the edge's flow

Our first application of the c.m.c.e. is to give an improved local flow as the initial data for Hildreth's scheme. First we give an improved model which is based on the Hildreth's original approach but consider the new local information from c.m.c.e..

In general, there will be error in both the local computation of $\mathbf{N} \cdot \mu$, which is denoted as $\mu^{\perp}$, and $\mathbf{T} \cdot \mu$ denoted as μ^{T}, which are caused by image quantisation and by image noise, etc. Therefore, in practice, we require that the flow only obey these local constraints approximately. Combining this approximate requirement with the general smoothness assumption along the edge direction, we have the following functional to be minimised:

$$\Theta = \int [(\frac{\partial \mu_x}{\partial s})^2 + (\frac{\partial \mu_y}{\partial s})^2] ds + \alpha \int [\mathbf{N} \cdot \mu - \mu^{\perp}]^2 ds + \beta \int [\mathbf{T} \cdot \mu - \mu^{\mathsf{T}}]^2 ds \tag{17}$$

Minimising the second and third terms in the above equation corresponds to the approximate requirement of local normal and tangential flow constraint, respectively. The parameter α is a weighting factor which expresses the degree of confidence in the local computation of normal flow from the m.c.e.. β is another weighting factor for the local tangential flow. We set α to be a constant along edges, but set β to be a function of the local Hessian matrix which is varying along the edge.

$$\beta = \frac{det\mathbf{H}}{\epsilon}$$

This function represents two aspects of error sources in the tangential flow computation, where ϵ expresses the degree of confidence in the computation of Hessian matrix itself, the determinant of Hessian represents the degree of confidence in using the c.m.c.e.. In general, ϵ should be the *condition number* of the Hessian matrix (see [2] for condition number of the matrix).

$$\epsilon = \|\mathbf{H}\| \|\mathbf{H}^{-1}\|$$

where ϵ equals to 1 corresponding to well-conditioned, and ∞ corresponding to singular. The smaller value of ϵ assocites with better conditioning which makes β bigger. Also, in general, β should be smaller than α, as the error in the computation of second order intensity derivatives are bigger than in the first order derivative's computation. The discrete functions for the first, second and third term in the functional of equation 17 are as follows:

$$\Theta_1 = \sum_{i=2}^{n} [(\mu_{x_i} - \mu_{x_{i-1}})^2 + (\mu_{y_i} - \mu_{y_{i-1}})^2] + [(\mu_{x_1} - \mu_{x_n})^2 + (\mu_{y_1} - \mu_{y_n})^2]$$

$$\Theta_2 = \alpha \sum_{i=1}^{n} [\mu_{x_i} N_{x_i} + \mu_{y_i} N_{y_i} - \mu_i^{\perp}]^2$$

$$\Theta_3 = \frac{det\mathbf{H}}{\epsilon} \sum_{i=1}^{n} [\mu_{x_i} T_{x_i} + \mu_{y_i} T_{y_i} - \mu_i^{\mathsf{T}}]^2$$

From Θ_1, Θ_2 and Θ_3, we have the discrete formula for equation 17 as:

$$\Phi = \Theta_1 + \Theta_2 + \Theta_3 \tag{18}$$

Now, the question of minimising equation 17 leads to the question of finding a set of x and y components of the flow, which minimise the discrete function Φ. This gives a set of $2n$ linear equations to be solved, which are:

$$\frac{\partial \Phi}{\partial \mu_{x_i}} = 0, \quad \frac{\partial \Phi}{\partial \mu_{y_i}} = 0, \quad 1 \le i \le n. \tag{19}$$

From the partial derivatives with respect to the x component of function Φ, we have:

$$\begin{aligned} &[4 + 2\alpha(N_{x_i})^2 + 2\frac{det\mathbf{H}}{\epsilon}(T_{x_i})^2]\mu_{x_i} - 2\mu_{x_{i+1}} \\ &-2\mu_{x_{i-1}} + [2\alpha N_{x_i} N_{y_i} + 2\frac{det\mathbf{H}}{\epsilon} T_{x_i} T_{y_i}]\mu_{y_i} \\ &= 2\alpha N_{x_i} \mu_i^{\perp} + 2\frac{det\mathbf{H}}{\epsilon} T_{x_i} \mu_i^{\mathsf{T}} \\ &1 \le i \le n. \end{aligned}$$

From the partial derivatives with respect to the y component of function Φ, we have:

$$\begin{aligned} &[4 + 2\alpha(N_{y_i})^2 + 2\frac{det\mathbf{H}}{\epsilon}(T_{y_i})^2]\mu_{y_i} - 2\mu_{y_{i+1}} \\ &-2\mu_{y_{i-1}} + [2\alpha N_{x_i} N_{y_i} + 2\frac{det\mathbf{H}}{\epsilon} T_{x_i} T_{y_i}]\mu_{x_i} \\ &= 2\alpha N_{y_i} \mu_i^{\perp} + 2\frac{det\mathbf{H}}{\epsilon} T_{y_i} \mu_i^{\mathsf{T}} \\ &1 \le i \le n. \end{aligned}$$

These two equations constitute an improved model relative to Hildreth's original scheme [7], [8]. It uses more local information both from the m.c.e. and the c.m.c.e. to give a faster algorithm.

5 Experimental results

In order to show that our model works on practical images, we show the results of some initial experiments. First we give some results which are for testing the c.m.c.e.. Secondly, we show some results from our improved version of Hildreth's algorithm.

We first explain the pictures been used. The aim of this part of the experiment is to show whether the equation works, based on the degree of curving on the edges which we have shown theoretically. Therefore, we try to use a kind of image which has less influence from other aspects, such as noise in the image which leads to errors in edge detection and so on. This leads us to use a sequence of synthetic ellipse images which has different curvature along its boundary. The image sequences include translation, rotation and deformation (figure 2). The size of the images is 128 × 128.

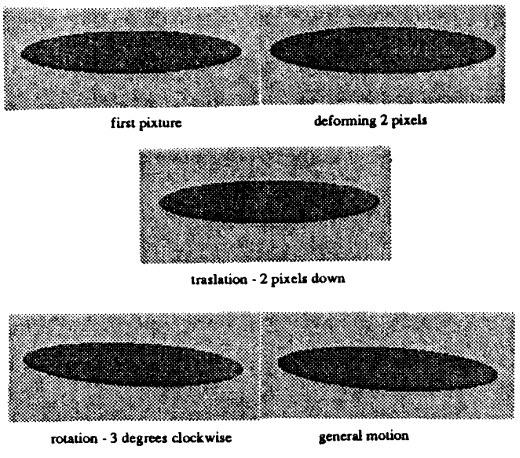

Figure 2: Synthetic image sequences for the experiment of c.m.c.e..

The flow fields are shown in figures 3, 4, 5 and 6. Each figure also shows a result from Hildreth's method, but all of them are about ten times slower. We note that most time consuming in the computation spends on computing all the derivatives for which we are using relatively large masks (7×7 and 9×9) because the computation of the second order derivatives are very sensitive in general. On the other hand, the computing time in Hildreth's method is mostly spent in the iteration stage which is inherently sequential. Therefore we can further speed up the seed motion computation considerably and easily by using a hardware image processing array. In figure 3, we have a translation in which the local normal flow of the loci of seed are useless. The recovered local tangential flow complement the local full flow rather well. This associates with the two extreme situations we mentioned before. Here, the tangential flow gives a reasonably accurate contribution to the full flow at the seed loci. Figure 4 gives a three degrees clockwise rotation and, figure 5 shows a motion of rotation in three degrees clockwise and translation of two pixels in both x and y directions. Finally, figure 6 has a flow associated with a motion of two pixels deforming in all directions. In the final two more general situations, the c.m.c.e still gives a quite reasonable local tangential flow.

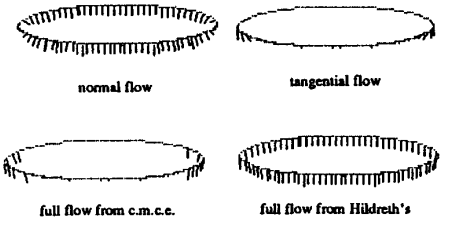

Figure 3: Synthetic translation — 2 pixels down the y direction.

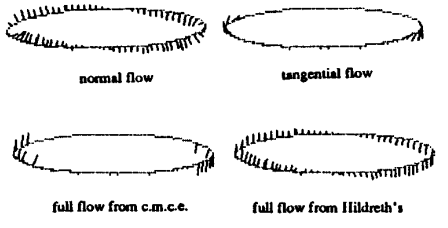

Figure 4: Synthetic rotation — 3° clockwise.

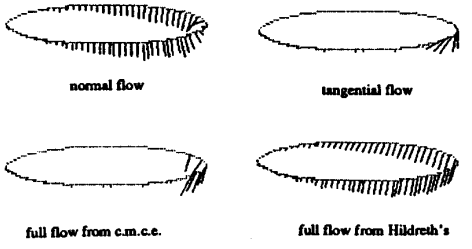

Figure 5: Synthetic general motion — translating 2 pixels in both x and y directions; also rotating 3° clockwise.

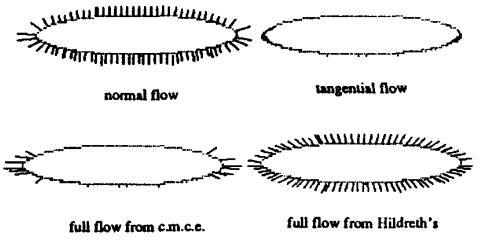

Figure 6: Synthetic deformation — 2 pixels in all directions.

We have demonstrated the adequacy on sequences of synthetic images. But these are images that have simple structure. For real images, the situation is different simply as, on one hand, there are lots of noises both from the original image, and from the image quantisation; and on the other hand, the computation of second order derivatives are well known to be sensitive to noise. Therefore, we consider the local tangential flow as an *approximate* local constraint for the full flow computation, as in equation 17 rather than as a precise calculation. The result from applying our improved Hildreth's method on the real image sequence is shown in figure 7. This result didn't show us a great change in the time consuming (about two third the iterations as Hildreth's does). The reason can be explained as there are not enough seeds along the edges; also we don't fix their tangential flow as boundary conditions which turns out that the seed's contributions are buried in or smoothed by the non-seed's normal flow. This leads to our following consideration of an alternative way for applying the c.m.c.e..

Currently, we compute a fairly good approximation to the local tangential flow at the seed loci, or we compute the tangential flow everywhere on the edge by setting the threshold of $det\mathbf{H}$ to zero, which will give us a very low confidence about the tangential flow at the loci of low $det\mathbf{H}$. Consequently, our current investigations start from finding how to build up the local tangential flow all along the edge by propagating, instead of directly computing from equation 14, the tangential flow at the loci of seed to the loci of low $det\mathbf{H}$. This should give us a more confident tangential flow at those loci of $det\mathbf{H}$. Although these propagated tangential flows along the edge still can only be approximate, they will have greater confidence. We are currently exploring the possibility of using wave-diffusion processing (based on the assumption that the change of tangential flow is continuous along the edge) to give us a fast propagation along the edge. This processing will again be inherently parallel. After we have the tangential flow everywhere on the edge, we combine them locally with the normal flow, to give us a very close approximation to this edgel's full flow. By this stage, we only need a few final iterations to smooth the whole flow globally to overcome the initial error that derives from *noise* rather than from *insufficient constraint*. In this way, we use the local computation as much as we can to minimise the involvement with the global computation. Therefore, most of our computation can be done in parallel. The reasons for doing so is to understand how we can propagate the reliable optic flow into less constrained regions and at the same time how much parallelism can be achieved. The ultimate goal is to understand the multi-level optic flow computation structure. Answering the questions such as how much parallelism is associated with a certain level's computation, how we can maximally apply it, and finally, how much parallelism is in the whole optic flow computation, will bring us to a better understanding of the parallel computation of visual motion.

Frame 1

Frame 2

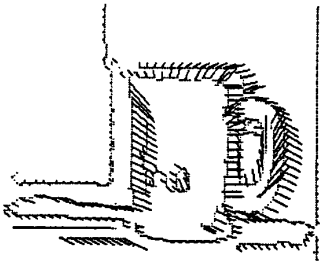

Figure 7: A cup in a general motion (include a rotation by the centre of the cup and a translation towards the lower right hand corner).

Acknowledgements

I thank my supervisor, Mike Brady, for very helpful discussions and suggestions. Also thanks to Bernard Buxton, David Murray, Guy Scott, Andrew Zisserman and all the others in the Vision Lab. for all the helps in various ways. The author acknowledges the support of the Royal Society and the GEC Hirst Research Laboratories.

Appendix

Before we start to derive equations 12 and 13, it is important to note the basic definitions in equations 2 and 4. We start from giving a few lemmas which are essential for our demanding result.

Lemma 1. if we assume that $\frac{ds}{dt} = (1/\frac{dt}{ds}) = const.$, which in general will be true, we have:

$$\frac{\partial \mu}{\partial s} = \frac{d\mathbf{T}}{dt} \tag{20}$$

Proof. From equations 2 and 4, we find:

$$\begin{aligned}\frac{\partial \mu}{\partial s} &= \frac{\partial}{\partial s}\left[\begin{array}{cc} dx/dt & dy/dt \end{array}\right]^{\top} \\ &= \left[\begin{array}{ccc} \partial^2 x/\partial s \partial t & + & \partial^2 x/\partial s^2 \cdot ds/dt \\ \partial^2 y/\partial s \partial t & + & \partial^2 y/\partial s^2 \cdot ds/dt \end{array}\right]\end{aligned}$$

$$\begin{aligned}\frac{d\mathbf{T}}{dt} &= \frac{d}{dt}\left[\begin{array}{cc} \partial x/\partial s & \partial y/\partial s \end{array}\right]^{\top} \\ &= \left[\begin{array}{ccc} \partial^2 x/\partial s \partial t & + & \partial^2 x/\partial s^2 \cdot ds/dt \\ \partial^2 y/\partial s \partial t & + & \partial^2 y/\partial s^2 \cdot ds/dt \end{array}\right]\end{aligned}$$

The lemma follows. □

Lemma 2. Along an edge as defined by $I_{xx} + I_{yy} = 0$,

$$-\left[\begin{array}{cc} I_{xy} & I_{yy} \\ -I_{xx} & -I_{xy} \end{array}\right]\mathbf{N} = \mathbf{HT} \tag{21}$$

and

$$\left[\begin{array}{cc} I_{xy} & I_{yy} \\ -I_{xx} & -I_{xy} \end{array}\right]\mathbf{T} = \mathbf{HN} \tag{22}$$

where H is the image Hessian

$$\mathbf{H} = \left[\begin{array}{cc} I_{xx} & I_{xy} \\ I_{xy} & I_{yy} \end{array}\right] \tag{23}$$

The proof of the lemma simply consists of expanding both sides of the equation. □

From lemma 2, it follows:

Lemma 3.

$$\|\nabla I\|\mathbf{N}\cdot\frac{d\mathbf{T}}{dt} + \frac{\partial I_t}{\partial s} = -\mathbf{T}^{\top}\mathbf{H}\mu \tag{24}$$

Proof. From the definition of gradient, we have:

$$\mathbf{N} = \frac{1}{\|\nabla I\|}\left[\begin{array}{c} I_x \\ I_y \end{array}\right] \tag{25}$$

As **T** is orthogonal to **N**, therefore:

$$\mathbf{T} = \frac{1}{\|\nabla I\|}\left[\begin{array}{c} I_y \\ -I_x \end{array}\right] \tag{26}$$

Taking partial derivatives with respect to s and t of equation 26, gives the following:

$$\frac{\partial\|\nabla I\|}{\partial s}\mathbf{T} + \|\nabla I\|\frac{\partial \mathbf{T}}{\partial s} = \left[\begin{array}{c} \partial I_y/\partial s \\ -\partial I_x/\partial s \end{array}\right]$$

$$\frac{\partial\|\nabla I\|}{\partial t}\mathbf{T} + \|\nabla I\|\frac{\partial \mathbf{T}}{\partial t} = \left[\begin{array}{c} \partial I_y/\partial t \\ -\partial I_x/\partial t \end{array}\right]$$

We now take scalar products with **N** in these two equations. From the second one, we have:

$$\frac{\partial \mathbf{T}}{\partial t} = -\frac{1}{\|\nabla I\|}(\mathbf{T}\cdot\nabla\mathbf{I_t})\mathbf{N} \tag{27}$$

Applying lemma 2 to the first equation, we have:

$$\begin{aligned}\|\nabla I\|\frac{\partial \mathbf{T}}{\partial s}\cdot\mathbf{N} &= \begin{bmatrix} I_{xy}(\partial x/\partial s)+I_{yy}(\partial y/\partial s) \\ -I_{xx}(\partial x/\partial s)-I_{xy}(\partial y/\partial s)\end{bmatrix}\cdot\mathbf{N} \\ &= \mathbf{T}\begin{bmatrix} I_{xy} & I_{yy} \\ -I_{xx} & -I_{xy}\end{bmatrix}\mathbf{N} \\ &= -\mathbf{T}^{\top}\mathbf{H}\mathbf{T}\end{aligned}$$

which gives,

$$\frac{\partial \mathbf{T}}{\partial s} = -\frac{1}{\|\nabla I\|}(\mathbf{T}^{\top}\mathbf{H}\mathbf{T})\mathbf{N} \tag{28}$$

Again, take partial derivatives with respect to x and y on both sides of equation 26, and then form scalar products with $\mathbf{N}$, we find:

$$\|\nabla I\|\frac{\partial \mathbf{T}}{\partial x}\cdot\mathbf{N} = \frac{1}{\|I\|}(I_{xy}I_x - I_{xx}I_y)$$

and

$$\|\nabla I\|\frac{\partial \mathbf{T}}{\partial y}\cdot\mathbf{N} = \frac{1}{\|I\|}(I_{yy}I_x - I_{xy}I_y)$$

These lead to:

$$\frac{\partial \mathbf{T}}{\partial x} = \frac{1}{\|\nabla I\|^2}(I_{xy}I_x - I_{xx}I_y)\mathbf{N} \tag{29}$$

$$\frac{\partial \mathbf{T}}{\partial y} = \frac{1}{\|\nabla I\|^2}(I_{yy}I_x - I_{xy}I_y)\mathbf{N} \tag{30}$$

Now, as:

$$\frac{d\mathbf{T}}{dt} = \frac{\partial \mathbf{T}}{\partial x}\frac{dx}{dt} + \frac{\partial \mathbf{T}}{\partial y}\frac{dy}{dt} + \frac{\partial \mathbf{T}}{\partial t}$$

Applying equations 27, 29 and 30 yield:

$$\frac{d\mathbf{T}}{dt} = -\frac{1}{\|\nabla I\|}(\mathbf{T}^{\top}\mathbf{H}\mu)\mathbf{N} - \frac{1}{\|\nabla I\|}(\mathbf{T}\cdot\nabla\mathbf{I_t})\mathbf{N} \tag{31}$$

Notice the notation for $\mathbf{T}$ before, equation 4, we derive the following straightforwardly.

$$\frac{\partial I_t}{\partial s} = \mathbf{T}\cdot\nabla\mathbf{I_t} \tag{32}$$

Equation 31 and 32 will give the lemma. □

Lemma 4.

$$\frac{\partial\|\nabla I\|}{\partial s} = \mathbf{T}^{\top}\mathbf{H}\mathbf{N} \tag{33}$$

Proof. As we have

$$\|\nabla I\|^2 = I_x^2 + I_y^2$$

Taking partial derivative with respect to s gives:

$$\begin{aligned}\|\nabla I\|\frac{\partial\|\nabla I\|}{\partial s} &= I_x\frac{\partial I_x}{\partial s} + I_y\frac{\partial I_y}{\partial s} \\ &= \|\nabla I\|(\mathbf{N}\cdot\begin{bmatrix}\partial I_x/\partial s \\ \partial I_y/\partial s\end{bmatrix})\end{aligned}$$

The lemma follows. □

Lemma 5.

$$\frac{\partial \mathbf{N}}{\partial s} = \frac{1}{\|\nabla I\|}(\mathbf{T}^{\top}\mathbf{H}\mathbf{T})\mathbf{T} \tag{34}$$

Proof. From the Frenet-Serret equations, we have:

$$\frac{\partial \mathbf{T}}{\partial s} = \kappa\mathbf{N} \tag{35}$$

$$\frac{\partial \mathbf{N}}{\partial s} = -\kappa\mathbf{T} \tag{36}$$

Substituting equation 28 into 35 will give:

$$\kappa = -\frac{1}{\|\nabla I\|}(\mathbf{T}^{\top}\mathbf{H}\mathbf{T})$$

Combining this with equation 36 completes the proof. □

From lemma 4 and 5, therefore:

Lemma 6.

$$\begin{aligned}\frac{\partial\nabla\mathbf{I}}{\partial s} &= \frac{\partial\|\nabla I\|}{\partial s}\mathbf{N} + \|\nabla I\|\frac{\partial \mathbf{N}}{\partial s} \\ &= (\mathbf{T}^{\top}\mathbf{H}\mathbf{N})\mathbf{N} + (\mathbf{T}^{\top}\mathbf{H}\mathbf{T})\mathbf{T} \\ &= \mathbf{H}\mathbf{T}\end{aligned} \tag{37}$$

□

By now, applying lemma 1, lemma 6 and equations 31, 32 into equation 10 will give us equation 12. In the same way, without equation 32, we can derive equation 13 from equation 11.

References

[1] J.M. Brady. Seeds of Perception. In *Proceedings of The Third Alvey Vision Conference*, pages 259–267, University of Cambridge, Cambridge, England, September 1987.

[2] G. Dahlquist and A. Bjorck. *Numerical Methods.* Prentice-Hall, Englewood Cliffs, N.J., 1974.

[3] L.S. Davis, Z. Wu, and Sun H. Contour Based Motion Estimation. *Computer Vision, Graphics and Image Processing*, 23:313–326, 1983.

[4] S.G Gong. Improved Local Flow. In *Proceedings of The Fouth Alvey Vision Conference*, pages 129–134, University of Manchester, Manchester, England, September 1988.

[5] S.G. Gong. *Parallel Computation of Visual Motion.* MSc. Report, Oxford University, England, July 1987.

[6] Haralick, R.M. Digital Step Edges from Zero-crossings of Second Directional Derivatives. *IEEE Trans. Pattern Anal. and Machine Intell.*, PAMI-6(1):58–68, 1984.

[7] E.C. Hildreth. Computations Underlining the Measurement of Visual Motion. *Artificial Intelligence*, 23(3):309–354, 1983.

[8] E.C. Hildreth. *The Measurement of Visual Motion.* MIT Press, Cambridge, Mass., 1984.

[9] B.K.P. Horn and B.G Schunck. Determining Optical Flow. *Artifical Intelligence*, 17:185–203, 1981.

[10] Koenderink, J.J. Optic Flow. *Vision Research*, 26(1):161–180, 1986.

[11] Koenderink, J.J. and Doorn, A.J. Invariant Properties of the Motion Parallax Field due to the Movement of Rigid Bodies Relative to An Observer. *Optica Acta*, 22(9):773–791, 1975.

[12] Koenderink, J.J. and Doorn, A.J. Local Structure of Movement Parallax of the Plane. *J. Opt. Soc. Am.*, 66(7):717–723, 1976.

[13] H.H Nagel. An Investigation of Smothness Constraints for the Estimation of Displacement Vector Fields from Image Sequences. *IEEE Trans. Pattern Anal. and Machine Intell.*, PAMI-8(5):565-593, 1986.

[14] H.H Nagel. Displacement Vectors Derived from Second Order Intensity Variations in Image Sequences. *Computer Vision, Graphics and Image Processing*, 21:85–117, 1983.

[15] H.H Nagel. On the Estimation of Optical Flow: Relations between Different Approaches and Some New Results. *Artifical Intelligence*, 33:299–324, 1987.

[16] J.A Noble. Morphological Feature Detection. In *Proceedings of The Fouth Alvey Vision Conference*, pages 203–208, University of Manchester, Manchester, England, September 1988.

[17] J.A. Noble. *The Geometric Structure of Images.* MSc. Report, Oxford University. July 1987.

[18] Ramachandran, V.S. Apparent Motion of Subjective Surfaces. *Perception*, 14:127–134, 1985.

[19] Ramachandran, V.S. and Anstis, S.M. Perceptual Organization in Multistable Apparent Motion. *Perception*, 14:135–143, 1985.

[20] G.L Scott. *Local and Global Interpretation of Moving Images.* PhD thesis, Cognitive Studies Program, University of Sussex, England, 1986.

[21] G.L Scott. *The Four Line Method of Locally Estimating Optical Flow.* Technical Report, University of Sussex, England, 1986.

[22] S. Ullman. *The Interpretation of Visual Motion.* MIT Press, Cambridge, Mass., 1979.

[23] A.M. Waxman, K. Behrooz, and S. Muralidhara. Closed-Form Solutions to Image Flow Equations for 3D Structure and Motion. *The International Journal of Computer Vision*, 1:239–258, 1987.

[24] A.M. Waxman and K. Wohn. Contour Evolution, Neighbourhood Deformation and Global Image Flow: Planar Surfaces in Motion. *The International Journal of Robotics Research*, 4(3):95–108, 1985.

[25] R.J. Woodham. Analysing Images of Curved Surfaces. *Artificial Intelligence*, 17:117–140, 1981.

[26] M. Yachida. Determining Velocity Maps by Spatio-Temporal Neighbourhoods from Image Sequences. *Computer Vision, Graphics and Image Processing*, 21:262–279, 1983.